Preprints.org

Article

Not peer-reviewed version

Microbial Bioleaching of Critical Metals from Spent Lithium-Ion Batteries: A Biohydrometallurgical Approach

Kyriaki Kiskira *, Lamprini-Areti Tsakanika, Aristides Kritikos, Konstantina Papadopoulou, Elias Chatzitheodoridis, Gerasimos Lyberatos, Maria Ochsenkühn-Petropoulou

Posted Date: 27 January 2026

doi: 10.20944/preprints202601.1942.v1

Keywords: bioleaching; *Acidithiobacillus ferrooxidans*; black mass; spent lithium-ion batteries; lithium cobalt oxide ($LiCoO_2$); critical metal recovery; WEEE recycling; sustainable metal extraction

Preprints.org is a free multidisciplinary platform providing preprint service that is dedicated to making early versions of research outputs permanently available and citable. Preprints posted at Preprints.org appear in Web of Science, Crossref, Google Scholar, Scilit, Europe PMC.

Copyright: This open access article is published under a Creative Commons CC BY 4.0 license, which permit the free download, distribution, and reuse, provided that the author and preprint are cited in any reuse.

Preprints.org (www.preprints.org) | NOT PEER-REVIEWED | Posted: 27 January 2026 doi:10.20944/preprints202601.1942.v1

Disclaimer/Publisher's Note: The statements, opinions, and data contained in all publications are solely those of the individual author(s) and contributor(s) and not of MDPI and/or the editor(s). MDPI and/or the editor(s) disclaim responsibility for any injury to people or property resulting from any ideas, methods, instructions, or products referred to in the content.

Article

Microbial Bioleaching of Critical Metals from Spent Lithium-Ion Batteries: A Biohydrometallurgical Approach

Kyriaki Kiskira [1,2]*, Lamprini-Areti Tsakanika [1], Aristides Kritikos [1], Konstantina Papadopoulou [3], Elias Chatzitheodoridis [4], Gerasimos Lyberatos [3] and Maria Ochsenkühn-Petropoulou [1]

[1] Laboratory of Inorganic and Analytical Chemistry, School of Chemical Engineering, National Technical University of Athens, Iroon Polytechniou 9, Zografou Campus, 15773 Athens, Greece

[2] Department of Industrial Design and Production Engineering, School of Engineering, University of West Attica, Campus 2 Thivon 250, 12241 Aigaleo, Greece

[3] Laboratory of Organic Chemical Technology, School of Chemical Engineering, National Technical University of Athens, Iroon Polytechniou 9, Zografou Campus, 15773 Athens, Greece

[4] Laboratory of Mineralogy, Petrology and Economic Geology,School of Mining and Metallurgical Engineering; National Technical University of Athens, Iroon Polytechniou 9, Zografou Campus, 15773 Athens, Greece

* Correspondence: kkiskira@uniwa.gr

Abstract

Biohydrometallurgical processing of spent lithium-ion batteries offers a low-impact route for critical metal recovery compared with conventional hydrometallurgy. In this work, the iron-oxidizing bacterium *Acidithiobacillus ferrooxidans* was evaluated for the bioleaching of cobalt (Co), nickel (Ni), lithium (Li) and copper (Cu) from the black mass of spent $LiCoO_2$ batteries. Batch experiments were conducted in 9K medium at 30 °C, varying pulp density (1-2 %, w/v), inoculum volume (10-20 mL in 200 mL medium) and initial pH (with and without adjustment). At 1 % pulp density and 10 % v/v inoculum, metal recoveries after 6-7 days reached about 64-70 % Co, 57-72 % Ni, 52-60 % Li and 81-100 % Cu, with most dissolution occurring in the first 6 days. Higher inoculum loads without initial pH adjustment increased Li recovery up to 79 %, but did not further improve Co and Cu, indicating a trade-off between microbial activity, metal toxicity and ferric iron availability. The temporal evolution of pH and metal dissolution is consistent with indirect redoxolysis by biogenic Fe^{3+} and sulfuric acid generated during ferrous iron and elemental sulfur oxidation. Overall, the results confirm the feasibility of *A. ferrooxidans*-assisted bioleaching as a green option for Co, Ni, Li and Cu recovery from spent $LiCoO_2$ batteries and provide operating windows for subsequent process optimization and scale-up.

Keywords: bioleaching; *Acidithiobacillus ferrooxidans*; black mass; spent lithium-ion batteries; lithium cobalt oxide ($LiCoO_2$); critical metal recovery; WEEE recycling; sustainable metal extraction

1. Introduction

Waste electrical and electronic equipment (WEEE) is one of the fastest-growing waste streams worldwide, driven largely by the rapid expansion of portable electronics and electric mobility [1,2]. Spent lithium-ion batteries (LIBs) form a critical fraction of WEEE, as they contain significant amounts of valuable and critical raw materials such as cobalt (Co), lithium (Li), and nickel (Ni), which are indispensable for modern energy technologies and are officially recognized as critical by the EU and other international bodies [3–5].

© 2025 by the author(s). Distributed under a Creative Commons CC BY license.

Preprints.org (www.preprints.org) | NOT PEER-REVIEWED | Posted: 27 January 2026 doi:10.20944/preprints202601.1942.v1

Conventional recycling of spent LIBs is currently dominated by pyrometallurgical and hydrometallurgical routes, as well as emerging electrochemical processes [6–10]. Pyrometallurgy typically employs high-temperature smelting to recover metallic alloys but is energy intensive and often associated with substantial gaseous emissions and complex off-gas treatment [11–13]. Hydrometallurgical processes based on strong mineral acids (e.g., H_2SO_4, HCl, HNO_3, H_3PO_4), reducing agents, and multi-step separation schemes (precipitation, solvent extraction, ion exchange) can achieve high recoveries and high purity products, but they require significant chemical inputs and generate secondary effluents that must be carefully managed [14–19]. Recently, electrochemical recycling has attracted attention as a potentially cleaner, electricity-driven alternative; however, it is still at an early development stage and often needs precise control and relatively pure feed streams [20,21].

At the same time, most conventional routes are optimized for specific battery chemistries and may not be easily adaptable to the increasingly diverse LIB compositions entering the waste stream, particularly those containing complex cathode materials such as lithium cobalt oxide (LCO) [3,7]. For LCO-based batteries, cobalt remains the primary economic driver for recycling, but the simultaneous recovery of Li and Ni is increasingly important to ensure resource efficiency and to support circular economy strategies for critical raw materials (CRMs) [4,6].

Bio-hydrometallurgy has therefore emerged as a promising ‘green’ alternative or complement to existing recycling practices, enabling metal solubilization under mild operating conditions through the metabolic generation of acids and oxidants [22–24]. Bioleaching, the most widely applied bio-hydrometallurgical approach, has been used extensively in mining and is now gaining traction for the treatment of industrial residues and the black mass of spent LIBs [1,22,25,26]. The efficiency of microbial metal solubilization depends strongly on the characteristics of the feed material and on the composition of the cultivation medium [27,28]. Different microbial groups contribute distinct lixiviants: acidophilic sulphur- and iron-oxidizing bacteria such as *Acidithiobacillus ferrooxidans* and *Acidithiobasillus thiooxidans* generate ferric iron and sulphuric acid, which are potent oxidants for transition-metal-bearing phases [29,30], while filamentous fungi such as *Aspergillus niger* and *Penicillium chrysogenum* produce organic acids that promote the complexation and mobilization of Co, Ni, Li and Cu from secondary resources [24,31,32].

For spent LCO batteries, acidophilic bacteria are of particular relevance, as they operate effectively at low pH and moderate temperatures, conditions that align with both the stability window of cobalt-rich oxides and the requirements of industrial bioleaching practice [33,34]. A wide range of biocatalysts, media formulations and operational strategies has been explored in the literature, but systematic optimization remains limited, particularly for real industrial black mass, whose composition, microstructure, and impurity profiles differ markedly from synthetic or laboratory-prepared materials [28,35,36]. Parameters such as pulp density, initial pH, temperature, redox potential, inoculum size, and availability of energy sources (Fe^{2+}, S^0) have been identified as key factors controlling bioleaching performance, but their interactions are still not fully understood for complex LIB residues [25,37].

From a process-engineering perspective, bioleaching offers several advantages over conventional physicochemical recycling routes [37,38]. Operation near ambient temperature and atmospheric pressure significantly reduces energy consumption compared with pyrometallurgical processes [11,22,39]. The metabolites generated by microbial activity are generally less hazardous and easier to manage than strong mineral acids, thereby lowering the risk of secondary environmental contamination [40,41]. In some cases, bioleaching can also provide partial selectivity toward specific metals or oxidation states, which may reduce downstream purification requirements. However, practical challenges remain, including slow kinetics compared with conventional hydrometallurgy, sensitivity of microbial cultures to toxic shock or contamination, and limitations in reactor scale-up and process control [42,43]. Recent studies have begun to address these limitations. For instance, Alipanah et al. [25] applied design-of-experiments methodologies and thermodynamic modeling to

© 2025 by the author(s). Distributed under a Creative Commons CC BY license.

Preprints.org (www.preprints.org) | NOT PEER-REVIEWED | Posted: 27 January 2026 doi:10.20944/preprints202601.1942.v1

optimize bacterial bioleaching of spent LIBs, demonstrating significant recovery of Li, Co, Ni, and Mn under well-tuned conditions.

Within this context, *Acidithiobacillus ferrooxidans* is an especially attractive biocatalyst for the bioleaching of LCO-derived black mass [25,29,44]. This acidophilic, chemolithoautotrophic bacterium derives energy from the oxidation of ferrous iron and reduced sulphur compounds, generating ferric iron and sulphuric acid that act as powerful oxidizing and acidifying agents for metal dissolution [25,44,45]. It grows optimally at 20-35 °C and pH 1.5-3.5, conditions that align with efficient LCO dissolution and with the elevated metal loadings typical of industrial black mass. Its ability to grow autotrophically via CO_2 fixation simplifies medium formulation and reduces contamination hazards in long-term operation [29,44,46].

The present study investigates the microbial bioleaching of Co, Ni, Li and Cu from LCO-derived black mass using *A. ferrooxidans* under controlled batch conditions. The effects of inoculum volume, pulp density and initial pH adjustment are examined to identify operational conditions that maximize cobalt dissolution while ensuring significant co-recovery of Ni and Li. Bacterial activity, pH evolution and metal concentrations are monitored throughout the leaching period to elucidate the relationships between microbial metabolism, acid generation, redox chemistry and dissolution kinetics. Post-leaching residues are characterized to assess changes in mineralogy and microstructure and to confirm the preferential removal of metal-bearing phases. Overall, this work contributes to the development of an environmentally benign bio-hydrometallurgical route for the recovery of critical metals from spent LIBs and provides mechanistic insight into the performance and limitations of *A. ferrooxidans* during the bioleaching of industrial black mass.

2. Materials and Methods

2.1. Materials

2.1.1. Spent LCO Black Mass

The feed material (black mass) used in this study originated from spent LCO batteries that had undergone industrial pre-treatment, including thermal processing (pyrolysis) and mechanical size reduction. The resulting black mass consists of cathode and anode active materials, current collector fragments, and other electrode components in a powder form with heterogeneous particle size distribution. Prior to use in bioleaching experiments, the material was homogenized by gentle mixing and stored in sealed containers at room temperature to avoid moisture uptake and contamination.

The elemental composition of the black mass was determined by acid digestion followed by Atomic Absorption Spectroscopy (AAS) analysis. Approximately 0.2 g of dry black mass was digested in an autoclave bomb using freshly prepared aqua regia (HCl:HNO_3 molar ratio 3:1; 9.6 mL HCl and 2.4 mL HNO_3), at 80 °C for 2 h under continuous stirring at 250 rpm to ensure complete dissolution. After cooling, the digest was filtered through blue-band filter paper, quantitatively transferred to a volumetric flask, and diluted to 25 mL with ultrapure water prior to analysis. Cobalt, nickel, copper, iron, zinc, manganese, and lithium concentrations were quantified, and metal contents (mg/kg) in the black mass were calculated using the dilution factor and the liquid-to-solid ratio employed.

2.1.2. Reagents

All solutions were prepared with ultrapure water (18.2 MΩ·cm) obtained from a Barnstead™ Easypure™ II system (Thermo Scientific, USA). Sulphuric acid (≥95 % w/w, TRACESELECT, Honeywell) was used for pH adjustment of media and leachates, as well as for preparation of the 5 M H_2SO_4 stock solutions employed in cultivation and 9K media. Analytical-grade chemicals used for the preparation of the cultivation medium (Medium 882, Leibniz-Institute DSMZ) and the iron-rich 9K bioleaching medium included $(NH_4)_2SO_4$, $MgCl_2{\cdot}6H_2O$, KH_2PO_4, $CaCl_2{\cdot}2H_2O$, KCl, K_2HPO_4,

© 2025 by the author(s). Distributed under a Creative Commons CC BY license.

Preprints.org (www.preprints.org) | NOT PEER-REVIEWED | Posted: 27 January 2026 doi:10.20944/preprints202601.1942.v1

$MgSO_4 \cdot 7H_2O$, $Ca(NO_3)_2$, $FeSO_4 \cdot 7H_2O$, and trace elements ($MnCl_2 \cdot 4H_2O$, $ZnCl_2$, $CoCl_2 \cdot 6H_2O$, H_3BO_3, Na_2MoO_4, $CuCl_2 \cdot 2H_2O$).

2.1.3. Microorganism

Bioleaching experiments were carried out using the acidophilic, chemolithoautotrophic bacterium *Acidithiobacillus ferrooxidans*, obtained as an active culture from the Leibniz Institute DSMZ - German Collection of Microorganisms and Cell Cultures (Braunschweig, Germany). This bacterium was selected based on previous studies demonstrating its effectiveness in metal bioleaching and cobalt recovery from secondary resources and spent LIBs, as well as its ability to use ferrous iron as an energy source and to thrive in highly acidic, metal-rich environments.

2.2. Characterization of Black Mass

2.2.1. X-Ray Fluorescence (XRF)

Elemental composition and major metal oxides in the black mass were determined by energy-dispersive X-ray fluorescence (ED-XRF) using an Epsilon 1 spectrometer (Malvern Panalytical Ltd., Malvern, UK) equipped with an Ag-anode X-ray tube operated at 50 kV and 1 mA and a high-resolution silicon drift detector (SDD). Approximately 4 g of black mass were pressed or loaded into sample cups, and spectra were collected for 30 min per sample to ensure adequate counting statistics. Quantification of major oxides such as CuO, Co_3O_4, NiO phases was carried out using the instrument software and appropriate calibration CRMs standards.

2.2.2. X-Ray Diffraction (XRD)

Crystalline phases present in the black mass before and after bioleaching were identified by *XRD* using a BRUKER D8 ADVANCE diffractometer (Bruker Corp., Karlsruhe, Germany) equipped with Cu-Kα radiation (λ = 1.5418 Å) and a LYNXEYE 1D position-sensitive detector. Measurements were performed at 40 kV and 40 mA over a 2θ range of 10-90°, with a step size of 0.05° and a total scan time of 30 min per sample. Diffraction patterns were evaluated to confirm the presence of $LiCoO_2$, $LiNiO_2$, and graphite in the initial black mass, as well as to assess residual phases in the solid residues after bioleaching.

2.2.3. Scanning Electron Microscopy (SEM) and Energy Dispersive Spectroscopy (EDS)

The microstructure and local elemental composition of black mass particles and bioleached residues were examined by SEM using a JEOL JSM-6380LV microscope (JEOL Ltd., Tokyo, Japan) operated at 20 kV, coupled with an INCA X-Sight EDS microanalysis system (Oxford Instruments). Samples were dried, mounted on aluminum stubs, and coated with a thin conductive layer (e.g., Au) before imaging. SEM images were recorded at various magnifications to visualize particle morphology, graphite matrix, and metal-rich grains, while point EDS spectra were used to quantify the relative abundances of Co, Ni, Fe, Al, Si, Ca, and other elements in selected particles.

2.3. Cultivation of Acidithiobacillus ferrooxidans

The cultivation protocol recommended by DSMZ for Medium 882 was followed, with minor adaptations. Three stock solutions, designated A, B, and C, were prepared and subsequently combined to obtain the final cultivation medium.

Solution A consisted of 950 mL of ultrapure water containing 132 mg $(NH_4)_2SO_4$, 53 mg $MgCl_2 \cdot 6H_2O$, 27 mg KH_2PO_4, and 147 mg $CaCl_2 \cdot 2H_2O$; the pH was adjusted to 2.3 with 5 M H_2SO_4, and the solution was dispensed into conical Erlenmeyer flasks, sealed with hydrophobic cotton and aluminum foil, and sterilized at 121 °C for 20 min. Solution B consisted of 50 mL of 0.1275 M H_2SO_4 (initial pH ≈ 1.2) containing 20 g $FeSO_4 \cdot 7H_2O$; it was similarly dispensed, sealed, and autoclaved at 121 °C for 20 min. Solution C, a trace element solution, was prepared by dissolving 76 mg

© 2025 by the author(s). Distributed under a Creative Commons CC BY license.

Preprints.org (www.preprints.org) | NOT PEER-REVIEWED | Posted: 27 January 2026 doi:10.20944/preprints202601.1942.v1

$MnCl_2 \cdot 4H_2O$, 68 mg $ZnCl_2$, 64 mg $CoCl_2 \cdot 6H_2O$, 31 mg H_3BO_3, 10 mg Na_2MoO_4, and 67 mg $CuCl_2 \cdot 2H_2O$ in 1000 mL of distilled water; flasks were sealed and sterilized at 112 °C for 30 min.

The final cultivation medium (1001 mL) was prepared by mixing 950 mL of Solution A with 50 mL of Solution B and adding 1 mL of Solution C, resulting in a solution with pH 2.3. This medium was distributed into five Erlenmeyer flasks (200 mL each) and inoculated with 1 mL of *A. ferrooxidans* suspension per flask. Flasks were sealed with hydrophobic cotton and aluminum foil and incubated at 30 °C in an orbital shaker-incubator (ES-20, Biosan LLC, Riga, Latvia) at 100-120 rpm for 5 days to allow microbial growth and activation. During incubation, the bacterium developed a biofilm-like layer at the bottom of the flasks, which progressively covered the base by the end of the 5-day period.

2.4. Bioleaching Medium and Experimental Design

An iron-rich 9K medium was used as the leaching medium to provide ferrous iron as the energy source for *A. ferrooxidans*. The medium was prepared in 1 L of ultrapure water and contained 3 g $(NH_4)_2SO_4$, 0.1 g KCl, 0.5 g K_2HPO_4, 0.5 g $MgSO_4 \cdot 7H_2O$, 0.01 g $Ca(NO_3)_2$, and 44.7 g $FeSO_4 \cdot 7H_2O$. After distribution into Erlenmeyer flasks, the medium was sterilized at 121 °C for 20 min; upon cooling, its natural pH (≈3.5) was adjusted to 2.5 using 0.5 M H_2SO_4 unless stated otherwise. The trace mineral solution was added from a sterile stock solution and was prepared by dissolving the following compounds in a 1.5 $g \cdot L^{-1}$ nitrilotriacetic acid disodium salt solution (quantities were reported in $g \cdot L^{-1}$): 1.00 NaCl, 0.50 $MnSO_4$, 0.10 $FeSO_4 \cdot 7H_2O$, 0.10 $CoCl_2 \cdot 6H_2O$, 0.10 $CaCl_2 \cdot 2H_2O$, 0.13 ZnCl, 0.01 $CuSO_4 \cdot 5H_2O$, 0.01 $AlK(SO_4)_2 \cdot 12H_2O$, 0.025 $Na_2MoO_4 \cdot 2H_2O$ and 0.01 H_3BO_3, as described in [23].

Bioleaching experiments were conducted to examine the influence of inoculum volume, pulp density, and initial pH on metal dissolution from LCO-derived black mass. All tests were carried out in 250 mL Erlenmeyer flasks containing 200 mL of leaching suspension and incubated in an orbital shaker at 30 °C and 120 rpm. Flasks were sealed with hydrophobic cotton and aluminum foil to minimize contamination while allowing gas exchange.

A range of inoculum volumes (10-20 % v/v) was tested in combination with two pulp densities: 1 % w/v (2 g black mass per 200 mL) and 2 % w/v. Most experiments were initiated at an adjusted initial pH of 2.0, achieved by adding H_2SO_4 depending on the medium volume. In addition, a separate set of experiments was performed without any pH adjustment, in which the natural initial pH of the 9K-black mass suspension (≈2.3-2.8) was recorded and subsequently monitored throughout the entire leaching period. This allowed systematic comparison between pH-controlled and non-adjusted conditions.

All leaching suspensions were made up to 200 mL after addition of inoculum and solid material. Incubation periods varied between 6 and 13 days depending on the tested conditions. Control tests without bacterial inoculum were conducted under identical conditions to distinguish between chemical leaching and biologically mediated dissolution. All bioleaching and control experiments were performed in triplicate to ensure reproducibility.

2.5. Microbial Growth Monitoring

A growth curve for A. ferrooxidans was established to link bacterial activity with bioleaching performance. For this purpose, 20 mL of activated bacterial culture were inoculated into 230 mL of fresh cultivation medium in an Erlenmeyer flask and incubated at 30 °C and 120 rpm. At selected time points (0, 5, 10, 20, 30, 40, 50, 60, 70, and 80 h), about 3 mL of suspension were withdrawn and the optical density (OD) was measured at 600 nm using a UV-Vis spectrophotometer (HachLange DR2800), with the blank set to the inoculation time (t = 0 h). The OD_{600} values increased from 0.014 at t = 0 to approximately 0.7 after 50 h and then stabilized, indicating that the culture had reached a stationary phase.

2.6. Bioleaching Experiments and Sampling

© 2025 by the author(s). Distributed under a Creative Commons CC BY license.

Preprints.org (www.preprints.org) | NOT PEER-REVIEWED | Posted: 27 January 2026 doi:10.20944/preprints202601.1942.v1

Bioleaching tests were carried out for total durations ranging from 6 to 13 days, depending on the experiment, with intermediate sampling to follow pH and metal recovery over time. Sampling points typically included after 1 h, 6h and daily or every second day. At each sampling time, 2 mL of leachate were withdrawn using sterile syringes, filtered through 0.22 µm syringe filters (nylon membrane, Uniflo), and appropriately diluted with ultrapure water before AAS analysis.

The pH of the suspensions was measured at each sampling point using a digital portable pH-meter MP125 (Mettler Toledo, Columbus, OH, USA), which was calibrated daily using standard buffer solutions. pH evolution was recorded for all experiments and used to interpret the relationship between acid production, bacterial activity, and metal dissolution.

Metal concentrations (Co, Ni, Li, Cu, Fe, Mn, Zn) in the leachates were determined by flame AAS using a VARIAN AA240FS instrument (Varian Inc., Palo Alto, CA, USA), equipped with a multi-element lamp system and an air-acetylene burner. The instrument operated over 185-900 nm, and calibration curves were prepared using external standard solutions at 0.5, 1, and 2 mg/L, diluted from certified stock standards (100 and 1000 mg/L). The typical sample consumption was 6 mL/min. Lithium was quantified in emission mode, and the typical sample consumption was 3-5 mL/min. Metal recoveries (%) were calculated by comparing the dissolved metal mass in the leachate to the initial metal content in the black mass determined by digestion and AAS, taking into account the sampling volumes and dilution factors.

2.7. Post-Leaching Solid Characterization

After completion of the bioleaching experiments, solids were separated from the leachates by filtration or centrifugation. Residues were washed with ultrapure water to remove adhering solution, dried under controlled temperature and humidity conditions, and stored in sealed containers for further analysis. Dried residues were analyzed by XRD and SEM-EDS as described above, to evaluate mineralogical and microstructural changes induced by bioleaching, as well as to assess residual metal-bearing phases and graphite content.

3. Results and Discussion

3.1. Chemical Composition and Microstructure of the Black Mass

3.1.1. AAS Quantification

The results of AAS analysis, show that the black mass contains approximately 202 g/kg Co, 59.4 g/kg Ni, and 37.2 g/kg Li, with lower concentrations of Cu (14.7 g/kg), Fe (14.9 g/kg), and Mn (3.5 g/kg). These values are characteristic of LCO-based cathode materials and confirm cobalt as the dominant economically valuable metal, followed by Ni and Li. This composition is consistent with LCO-based cathode chemistries and with reported black mass compositions from industrial pre-treatment lines, where $LiCoO_2$ and $LiNiO_2$ coexist with graphite, current collector fragments and process-derived impurities [3,6,7,35,36]. The relatively high Co content confirms that cobalt remains the principal economic driver for the recycling of this type of LIBs, while the presence of Ni and Li justifies efforts toward their co-recovery [1,3,6,7].

3.1.2. XRF Results

XRF analysis was performed to obtain a semi-quantitative elemental profile of the inorganic fraction. The results are shown in Table 1, expressed both as elemental concentrations and corresponding metal oxides.

Table 1. XRF analysis of the black mass.

Element (Metal Oxide)	Element Concentration (%)	Metal Oxide Concentration (%)
Co (Co_3O_4)	19.1	26.3

© 2025 by the author(s). Distributed under a Creative Commons CC BY license.

Preprints.org (www.preprints.org) | NOT PEER-REVIEWED | Posted: 27 January 2026 doi:10.20944/preprints202601.1942.v1

Ni (NiO)	4.9	7.2
Cu (CuO)	0.8	1.0
Fe (Fe_2O_3)	0.8	1.2
Al (Al_2O_3)	0.6	1.0
Mn (MnO)	0.4	0.6
LOI	40%	

The XRF data confirm Co as the dominant metal species in the inorganic fraction, followed by Ni and Co. Li is absent from the spectrum due to its low atomic number (Z = 3), which results in low-energy X-ray emission that lies below the detector's sensitivity. Notably, the Co concentration measured by XRF (19.1 wt%) aligns closely with the AAS-derived value (20.2 wt%), and the Co:Ni ratios obtained by both methods (XRF ≈ 3.8; AAS ≈ 3.4) show strong agreement. This reinforces the reliability of the combined analytical approach. The 40% LOI reported in Table 1 corresponds to moisture, graphite, polymeric binders, carbonates, hydroxides, and other volatile or combustible species. After removal of this volatile fraction, approximately 60% of the black mass is inorganic and metal-bearing, consistent with thermally pre-treated LIB black mass reported in literature.

3.1.3. XRD Analysis of the Black Mass

The crystalline phases present in the spent LCO black mass were identified by XRD (Figure S1a). Analysis reveals distinct reflections associated with the active cathode materials $LiCoO_2$ and $LiNiO_2$, as well as the anode material graphite, and minor contributions from metallic current-collector components. $LiCoO_2$ is characterized by a prominent peak at 2θ ≈ 19°, with additional reflections at approximately 37.5°, 39.5°, 45.3° and 49.5°, whereas $LiNiO_2$ exhibits its primary peak at 18.8° alongside secondary reflections at 36.9°, 38.9° and 44.5°. The higher intensity of $LiCoO_2$ peaks compared with $LiNiO_2$ is consistent with the compositional data (Table 1), confirming that cobalt-bearing phases dominate the cathode fraction. Both $LiCoO_2$ and $LiNiO_2$ exhibit characteristic diffraction features of layered rhombohedral $R\bar{3}m$ structures, which is typical for stoichiometric and Li-deficient LCO-type oxides used in commercial LIBs. The most intense reflection in the diffractogram occurs at 2θ ≈ 26.6°, corresponding to the (002) plane of graphite, reflecting the high abundance of graphitic carbon originating from the anode. Additional graphite reflections at 38.9°, 44.6° and 54.7° confirm the presence of a highly crystalline hexagonal graphite phase. The dominance of the graphite peak is expected given that pyrolyzed industrial black mass retains anode carbon almost quantitatively. Weak reflections attributable to Cu and Al were also detected, originating from fragmented current collectors, an observation consistent with industrial pre-treatment studies of LCO battery waste [7,35,36].

The XRD patterns of the bioleached residues reveal pronounced changes compared to the initial black mass (Figure S1b). The most intense diffraction peak, located at approximately 26° (2θ), is attributed to graphite, originating from the black mass and remaining in the solid residue after bioleaching. However, the reduced apparent intensity of this graphite reflection relative to the initial material is likely not due to graphite dissolution, but rather to (i) surface coverage or partial encapsulation of graphite particles by secondary precipitates and (ii) an increase in the amorphous fraction of the residue, which is reflected by an elevated background and increased noise in the diffractogram. In addition, several diffraction features indicate the presence of hydrated iron sulfate phases in the residue. These are evidenced by a characteristic doublet around 28–29° (2θ), as well as additional reflections near 15° and 17° (2θ). The formation of such Fe-sulfate precipitates is consistent with bioleaching conditions and can significantly affect the relative intensities of crystalline phases by partially masking underlying reflections, including those of graphite. Notably, cobalt oxide phases are not detected in the bioleached residue. This absence is attributed to the effective dissolution of cobalt-containing phases during bioleaching. Any remaining cobalt-bearing compounds are expected to be present only in trace amounts, below the detection limit of XRD. Overall, the XRD results indicate that bioleaching leads to the selective removal of metal-bearing phases, while the solid residue is dominated by graphite and secondary iron sulfate precipitates with a partially amorphous

© 2025 by the author(s). Distributed under a Creative Commons CC BY license.

Preprints.org (www.preprints.org) | NOT PEER-REVIEWED | Posted: 27 January 2026 doi:10.20944/preprints202601.1942.v1

character. Such behavior is well documented in biohydrometallurgical leaching of LCO-based cathodes at Fe-rich conditions [6,9,14,22,25,28].

3.1.4. SEM-EDS Microstructural Analysis

Representative SEM images of the untreated black mass (Figure 1a,b,c) reveal a heterogeneous assemblage of angular, irregularly shaped particles embedded within a graphite-rich matrix. EDS spot analyses confirm the presence of Co-rich and Ni-rich grains corresponding to residual cathode coatings, as well as Cu-rich fragments associated with shredded current collector foils. The mixture of particle morphologies and compositions is characteristic of pyrolyzed industrial black mass, where mechanical liberation is incomplete and composite particles persist.

Following bioleaching, significant morphological changes are evident in the solid residues (Figure 1d,e,f). Surfaces of Co- and Ni-bearing particles appear etched, displaying increased roughness and porosity. Many particles exhibit partial dissolution fronts, consistent with oxidative removal of metal oxides. In parallel, graphite lamellae appear cleaner and more exposed, reflecting the preferential dissolution of active cathode phases while the carbon matrix remains largely intact.

EDS spectra of leached particles show a marked reduction in Co and Ni signals, with a corresponding relative enrichment of C, further confirming selective leaching of metal oxides. This microstructural evolution is advantageous for downstream processing, as it facilitates the physical separation, purification, or potential direct reuse of the recovered graphite fraction. Similar transformations during microbial or chemical leaching of spent LIBs have been widely reported and are considered beneficial for integrated recycling schemes [22,28,36,40].

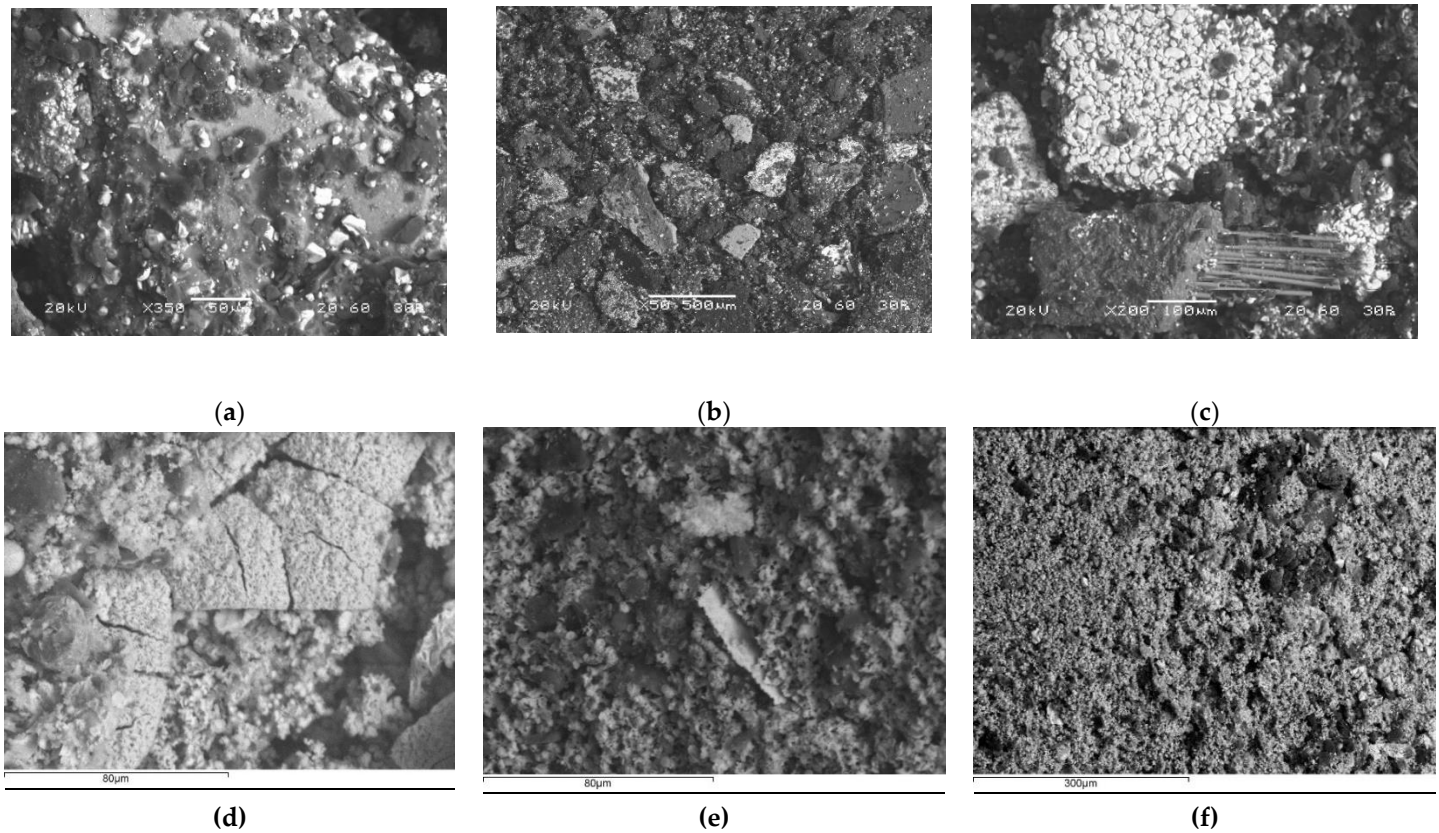

Figure 1. SEM micrographs of the spent LCO black mass before and after bioleaching. (**a-c**) Untreated black mass, showing heterogeneous agglomerates of angular Co- and Ni-rich particles embedded within a graphite matrix, together with Cu-rich fragments from current collectors; (**d-f**) Bioleached residues, exhibiting etched and porous surfaces, diminished Co/Ni-rich domains, and increasingly exposed graphite lamellae, indicating selective dissolution of metal-bearing phases by *A. ferrooxidans.*

© 2025 by the author(s). Distributed under a Creative Commons CC BY license.

Preprints.org (www.preprints.org) | NOT PEER-REVIEWED | Posted: 27 January 2026 doi:10.20944/preprints202601.1942.v1

3.2. Growth Behaviour of A. ferrooxidans and Implications for Bioleaching

The growth curve of *A. ferrooxidans* in the modified 882 medium is shown in Figure 2. After inoculation, the culture exhibited a short lag phase, followed by a rapid increase in OD_{600} from 0.014 to approximately 0.7 within 50 h, after which the optical density stabilized, indicating entry into the stationary phase. This behaviour is typical of iron-oxidizing acidophiles, where cell growth is tightly coupled to the oxidation of Fe^{2+} to Fe^{3+} and to the availability of dissolved oxygen [22,28,29,38].

The timing of the exponential growth phase is particularly relevant for the bioleaching experiments, since it coincides with the period of most intense Fe^{2+} oxidation and ferric iron regeneration. Operating the leaching tests at 30 °C and pH 2.0 ensures that the bacterium remains close to its optimal growth window [29,34,41,43]. The inoculum volumes employed in this study corresponding to 10-20 % v/v) thus provided a range of initial cell densities high enough to rapidly establish an active Fe^{2+}-oxidizing population while allowing evaluation of the effect of biomass load on leaching performance.

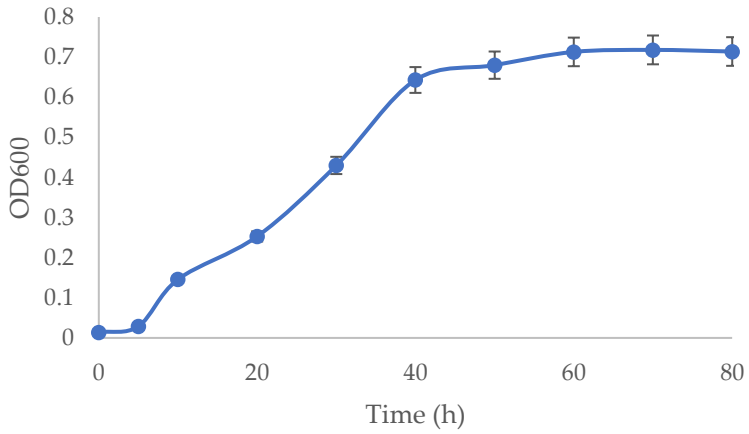

Figure 2. Growth curve of *Acidithiobacillus ferrooxidans* in modified 882 medium, expressed as optical density at 600 nm (OD_{600}) as a function of incubation time.

3.3. Effect of Inoculum Volume at 1 % Pulp Density

The influence of inoculum volume on metal dissolution was assessed at a pulp density of 1 % w/v (2 g black mass per 200 mL) and an initial pH of 2.0. Figure 3a,b,c presents the dissolution profiles of Co, Ni, Li and Cu for inoculum volumes of 10, 15 and 20 % v/v, respectively, while Figure 3d illustrates the effect of increasing pulp density to 2 % at 20 % v/v inoculum.

At 10 % v/v inoculum (Figure 3a), metal dissolution proceeded progressively over time, with most metals showing a pronounced increase up to day 6, followed by a slight additional increase by day 7. After 6-7 days, recoveries reached approximately 60-65 % for Co, 55-60 % for Ni, 50-55 % for Li, and 90 % for Cu, indicating efficient solubilization of readily accessible metal-bearing phases.

Increasing the inoculum volume to 15 % v/v (Figure 3b) resulted in moderately enhanced dissolution kinetics for all metals, particularly during the early stages of leaching. Final recoveries after 7 days increased to approximately 65-70 % for Co, 60-65 % for Ni, 70-75 % for Li, and 80-85 % for Cu. Li exhibited the most pronounced improvement with increasing inoculum volume, suggesting a strong dependence on microbial activity and acid generation.

At 20 % v/v inoculum (Figure 3c), metal recoveries followed a similar temporal trend, with rapid dissolution up to day 6 and marginal gains thereafter. Final recoveries after 7 days were comparable to those obtained at 15 % v/v, reaching approximately 60-65 % for Co, 55-60 % for Ni, 75-80 % for Li, and 80-85 % for Cu. The limited improvement relative to 15 % v/v indicates diminishing returns at

© 2025 by the author(s). Distributed under a Creative Commons CC BY license.

Preprints.org (www.preprints.org) | NOT PEER-REVIEWED | Posted: 27 January 2026 doi:10.20944/preprints202601.1942.v1

higher inoculum loadings, likely due to increased competition for ferrous iron, oxygen limitation, or metal toxicity effects.

Overall, these results indicate that moderate inoculum volumes (10-15 % v/v) are sufficient to sustain effective Fe^{2+} oxidation and metal dissolution at 1 % pulp density. Further increases in inoculum volume do not lead to proportional gains in recovery and may impose unnecessary biomass demand. Similar trends have been reported in other bioleaching studies of spent LIBs, where higher inoculum densities accelerate early leaching but have a limited effect on final metal recoveries [22,25,27–29,34,37,40].

3.4. Effect of Pulp Density

The influence of pulp density on bioleaching performance was evaluated by increasing the solids loading from 1 % to 2 % w/v (2 to 4 g black mass per 200 mL) while maintaining a constant inoculum volume (20 % v/v) and initial pH (2.0). The corresponding dissolution profiles are shown in Figure 3d, with results at 1 % pulp density provided for comparison in Figure 3a-c.

At 2 % pulp density, all target metals exhibited slower dissolution rates and substantially lower final recoveries than those obtained at 1 %. After 6-7 days of leaching, Co recovery decreased from approximately 64-70 % at 1 % pulp density to 35-45 %, while Ni and Li recoveries were reduced to similar extents. Copper dissolution was likewise inhibited, with final recoveries remaining below those observed under lower solids loading. The consistently lower slopes of the recovery curves in Figure 3d indicate that the inhibition occurs throughout the leaching period rather than only at later stages.

This behaviour reflects the intrinsic limitations imposed by higher solids loading in batch bioleaching systems. Increasing the pulp density raises the concentration of dissolved metals in the leachate, which can suppress microbial activity and slow ferric iron regeneration through inhibitory effects on *A. ferrooxidans* [22,28,34,43]. Simultaneously, the amount of ferrous iron supplied by the 9K medium becomes insufficient relative to the increased mass of solid, reducing the availability of ferric iron required for indirect oxidative dissolution. Higher pulp density also increases slurry viscosity and particle-particle interactions, which can impair oxygen transfer and limit effective contact between the biogenic lixiviants and metal-bearing phases.

Comparable reductions in bioleaching efficiency with increasing pulp density have been widely reported for spent LIB black mass, with most batch studies identifying optimal solids loadings at or below 1-2 % w/v to balance metal recovery and microbial stability [22,25,27,28,30,31,40,41]. The results obtained here are therefore consistent with literature trends and highlight pulp density as a critical design parameter that must be carefully controlled when translating bioleaching processes from laboratory to larger-scale systems.

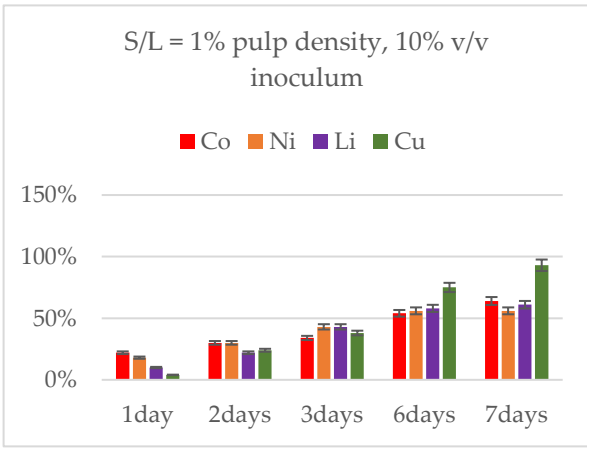

(**a**)

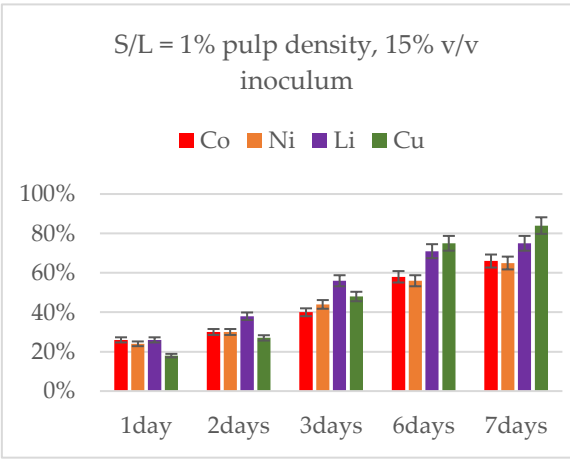

(**b**)

© 2025 by the author(s). Distributed under a Creative Commons CC BY license.

Preprints.org (www.preprints.org) | NOT PEER-REVIEWED | Posted: 27 January 2026 doi:10.20944/preprints202601.1942.v1

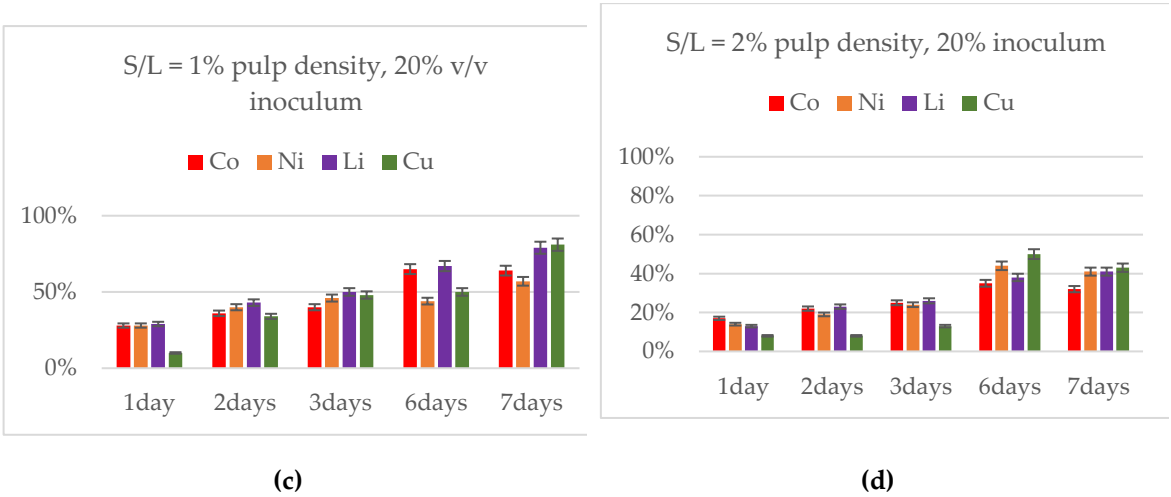

(c) **(d)**

Figure 3. Effect of inoculum volume and pulp density on bioleaching performance of spent LCO black mass. Metal recovery profiles of Co, Ni, Li and Cu at 30 °C and initial pH 2.0 for (**a**) 1 % pulp density and 10 % v/v inoculum, (**b**) 1 % pulp density and 15 % v/v inoculum, (**c**) 1 % pulp density and 20 % v/v inoculum, and (**d**) 2 % pulp density and 20 % v/v inoculum.

3.5. Influence of Initial and Dynamic pH Evolution on Bioleaching Performance

To elucidate the role of pH in controlling microbial activity and metal dissolution, bioleaching experiments were conducted either with initial pH adjustment to 2.0 or without adjustment, allowing the natural pH of the 9K-black mass suspension (≈2.3-2.8) to evolve freely. The temporal variation of pH during representative experiments is shown in Figure 4, corresponding to tests performed at 1 % pulp density with inoculum volumes of 10 % v/v (П1.5), 15 % v/v (П1.10) and 20 % v/v (П1.20).

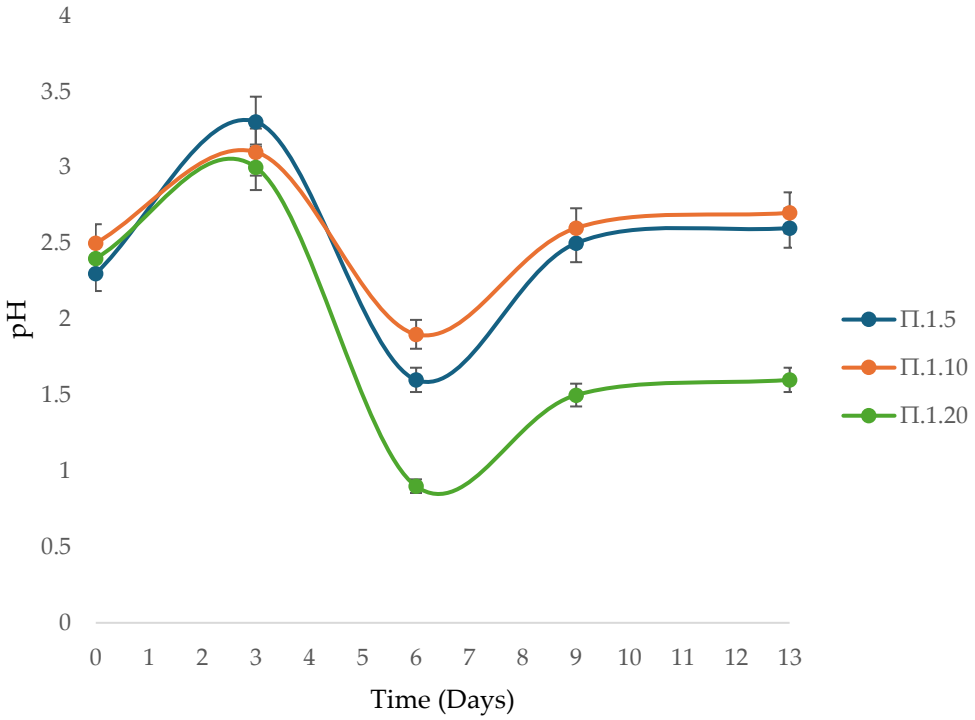

Figure 4. Temporal evolution of pH during bioleaching of spent LCO black mass by *Acidithiobacillus ferrooxidans* at 1 % pulp density. pH variation as a function of time for experiments conducted with different inoculum volumes: П1.5 (10 % v/v inoculum), П1.10 (15 % v/v inoculum) and П1.20 (20 % v/v inoculum). All experiments

© 2025 by the author(s). Distributed under a Creative Commons CC BY license.

Preprints.org (www.preprints.org) | NOT PEER-REVIEWED | Posted: 27 January 2026 doi:10.20944/preprints202601.1942.v1

were performed in 9K medium at 30 °C under shaking conditions, illustrating the influence of inoculum load on acidification dynamics during the bioleaching process.

In all pH-adjusted experiments, a characteristic pH profile was observed. During the first 2-3 days, pH increased slightly, reaching values around 3.0-3.3, reflecting initial buffering by the black mass and partial consumption of acidity during early metal dissolution. This was followed by a pronounced decrease in pH, reaching minimum values of approximately 1.5-1.6 for П1.5, ~1.9 for П1.10, and as low as ~0.9 for П1.20 around days 5-6. The subsequent gradual increase and stabilization of pH toward the end of the experiments (days 9-13) indicate partial neutralization as readily leachable phases were depleted and the rate of acid generation slowed.

This pH evolution is consistent with the indirect bioleaching mechanism mediated by *A. ferrooxidans*, in which oxidation of Fe^{2+} to Fe^{3+} and reduced sulphur compounds generates sulphuric acid, while ferric iron is simultaneously consumed during reductive dissolution of $LiCoO_2$ and $LiNiO_2$ phases [22,25,29,38,47]. The lowest pH values coincided with the period of most intense metal dissolution, indicating that acidification and ferric iron regeneration act synergistically to control leaching kinetics.

The magnitude of pH decrease was strongly dependent on inoculum volume. At 20 % v/v inoculum, rapid establishment of an active microbial population led to accelerated acid generation and the lowest pH values, whereas lower inoculum volumes resulted in more moderate acidification. This behaviour explains the faster initial dissolution observed at higher inoculum loadings, but also highlights the potential for excessively low pH to enhance metal toxicity or destabilize microbial activity over extended periods.

Experiments conducted without initial pH adjustment followed a similar qualitative trend but exhibited a more gradual acidification and did not reach the extremely low pH values observed in the adjusted systems. Under these conditions, final recoveries of Co, Ni and Cu remained comparable to those obtained at initial pH 2.0, demonstrating that *A. ferrooxidans* is capable of self-acidifying the system to levels sufficient for effective dissolution. Notably, Li recovery was consistently enhanced in the non-adjusted experiments, reaching values up to ~79 %, suggesting that slightly higher pH conditions may limit Li reprecipitation and favour proton-lattice exchange reactions [22,25,28,33,40].

The close correspondence between pH minima and the steepest increases in metal recovery confirms that pH evolution is a central process variable governing bioleaching efficiency, rather than a passive parameter. Together, these results indicate that strict initial pH adjustment is not mandatory for efficient Co and Ni recovery at low pulp density, but that controlled pH trajectories can be exploited to optimize Li dissolution and balance microbial activity against metal toxicity.

Overall, the data demonstrate that both initial pH conditions and dynamic pH evolution during leaching play a decisive role in determining bioleaching performance. Similar sensitivity of LIB bioleaching systems to pH and redox conditions has been widely reported for bacterial and mixed-culture processes treating LCO- and LFP-type cathode materials [22,28,30,43].

3.6. Linking pH Evolution, Microbial Activity and Dissolution Kinetics

The combined pH trajectories (Figure 4), growth behaviour (Figure 2), and dissolution curves (Figure 3) indicate that bioleaching performance was governed by the establishment of an active Fe^{2+}-oxidizing population and the resulting evolution of acidity and oxidative capacity in the leaching liquor. The rapid increase in OD_{600} up to ~50 h (Figure 2) marks the period during which Fe^{2+} oxidation and Fe^{3+} regeneration are expected to be most intense, supporting the indirect mechanism in which biogenic Fe^{3+} and acidity drive dissolution of $LiCoO_2$/$LiNiO_2$ phases [22,25,29,38,47]. Consistent with this, the steepest increases in metal recovery occurred during the interval of strongest acidification (Figure 4) and preceding the plateau observed after ~6-7 days (Figure 3), suggesting that dissolution was fastest while ferric regeneration and acidity build-up were highest.

As leaching progressed, recoveries approached a plateau and pH gradually stabilized, indicating a transition from an initially reaction-controlled regime (high availability of reactive

© 2025 by the author(s). Distributed under a Creative Commons CC BY license.

Preprints.org (www.preprints.org) | NOT PEER-REVIEWED | Posted: 27 January 2026 doi:10.20944/preprints202601.1942.v1

surfaces and strong oxidizing conditions) toward a regime limited by reduced accessibility of remaining metal-bearing phases. Such late-stage limitations are commonly attributed to depletion of readily leachable cathode material, surface passivation by altered layers, and/or diffusion constraints within composite particles, rather than simply insufficient biomass [28,34,43]. In this context, the pH history becomes a useful proxy for process intensity: pronounced acidification indicates sustained microbial oxidation activity, whereas stabilization reflects declining net acid generation and lower effective oxidative driving force.

3.7. Post-Leaching Residue Characterization

Mineralogical and microstructural analyses indicate the selective removal of metal-bearing cathode phases, while the carbonaceous component of the black mass remains in the solid residue. The XRD patterns of the leached residues (Figure S1b) show a pronounced attenuation of $LiCoO_2$ and $LiNiO_2$ reflections, consistent with the effective dissolution of Co- and Ni-containing oxides during bioleaching. The characteristic graphite reflection at ~26° (2θ) is still observed, confirming the persistence of graphitic carbon; however, its apparent intensity is reduced relative to the initial material, rather than remaining unchanged. This reduction is attributed to partial surface coverage or encapsulation of graphite particles by secondary precipitates, as well as to an increased proportion of amorphous phases in the residue, which manifests as an elevated background and increased noise in the diffractograms. Consequently, changes in relative peak intensities reflect not only phase abundance but also microstructural and surface effects induced during leaching. In several residues, weak reflections assignable to Fe-containing secondary phases were detected, consistent with the precipitation of hydrated iron sulfate species under acidic, Fe-rich bioleaching conditions. The formation of such secondary Fe phases is commonly reported in iron-driven bioleaching systems and may modify local surface chemistry and redox cycling, while not necessarily inhibiting overall metal dissolution. The absence of detectable crystalline cobalt phases further supports the conclusion that cobalt was effectively mobilized during bioleaching, with any remaining Co-bearing species present only at trace levels below the detection limit of XRD.

SEM observations further support this interpretation. Compared with the heterogeneous, compact agglomerates of the feed (Figure 1a-c), the bioleached residues (Figure 1d-f) exhibit etched surfaces, increased porosity and partial loss of Co/Ni-rich domains. The relative exposure of graphite lamellae and enrichment of carbon signatures in EDS are consistent with preferential dissolution of metal oxides and persistence of carbon-rich phases [22,28,36,40]. This residue evolution is relevant from a process perspective because it suggests that bioleaching can serve as a conditioning step that not only solubilizes target metals but also improves the liberation and potential valorization of the graphite fraction, depending on downstream separation routes.

3.8. Comparison with Previous Bioleaching Studies and Process Implications

A direct comparison between the present results and representative bioleaching studies reported in the literature is provided in Table 2. Under the best-performing conditions identified here (industrial LCO-derived black mass, 1 % pulp density, 30 °C, 6-7 days), Co and Ni recoveries of 64-70 % and 57-72 %, respectively, fall within the upper range typically reported for single-strain *Acidithiobacillus ferrooxidans* systems treating complex LIB residues. Li recovery reached 52-60 % under pH-adjusted conditions and increased up to approximately 79 % when the system was allowed to self-acidify, highlighting the sensitivity of Li behaviour to pH trajectories. Co dissolution was consistently high (81-100 %), reflecting the high lability of current-collector-derived Cu phases in acidic, oxidizing leachates and the effectiveness of the applied pretreatment.

Compared with fungal systems and mixed microbial consortia, which often require longer residence times or higher organic acid production to achieve comparable recoveries, the present results demonstrate that a single, well-characterized iron-oxidizing bacterium can deliver competitive performance on heterogeneous, pyrolyzed industrial black mass. This is notable given that such materials are typically more impurity-rich and structurally complex than laboratory-

© 2025 by the author(s). Distributed under a Creative Commons CC BY license.

Preprints.org (www.preprints.org) | NOT PEER-REVIEWED | Posted: 27 January 2026 doi:10.20944/preprints202601.1942.v1

prepared cathode powders, conditions that frequently suppress apparent bioleaching efficiency and slow dissolution kinetics.

Recent process-intensification approaches, including ultrasonic assistance and magnetic-field-enhanced bioleaching, have shown that higher recoveries or shorter leaching times can be achieved, particularly at elevated pulp densities. However, these configurations introduce additional operational complexity and energy inputs. In contrast, the present work establishes a robust baseline using a conventional shake-flask configuration and an unadapted *A. ferrooxidans* culture, demonstrating that substantial Co, Ni, Li and Cu recovery can be achieved under mild conditions without auxiliary intensification.

From a process perspective, the observed dissolution plateau after approximately 6-7 days suggests that staged leaching, liquor renewal or continuous operation may further enhance overall recovery by sustaining ferric iron regeneration and limiting late-stage inhibition. The strong dependence of performance on pulp density and pH evolution reinforces the need for careful control of solids loading, redox balance and acidification pathways during scale-up. Overall, these findings confirm the technical feasibility of *A. ferrooxidans*-assisted bioleaching for industrial LCO black mass and provide clear operational windows for subsequent optimization and integration into circular recycling flowsheets for spent lithium-ion batteries.

Table 2. This is a table. Tables should be placed in the main text near to the first time they are cited.

Study	Microorganism	Feed material	Key operating conditions	Co (%)	Ni (%)	Li (%)	Cu (%)
Heydarian et al., 2018 [34]	Mixed acidophilic culture	Laptop LIBs (mixed cathodes)	1% pulp, pH 1.8-2.0, 30 °C, two-step	~65	~55	—	—
Nazerian et al., 2023 [37]	*A. ferrooxidans* (+ ultrasound)	Spent LIB black mass	2% pulp, pH 2.0, 30 °C, ultrasound-assisted	68	62	71	—
Alipanah et al., 2023 [25]	*A. ferrooxidans*	Spent LIBs (mixed cathodes)	1% pulp, pH 2.0, 30 °C, optimized via DoE	~70	~60	~65	—
Panda et al., 2024 [27]	Mixed bacterial consortium	Industrial LIB black mass	1-2% pulp, pH 2.0, 30 °C, scale-up tests	60-68	55-63	50-65	—
Kim et al., 2024 [45]	*A. ferrooxidans* + magnetic field	Spent LIB cathode material	3% pulp, pH 2.0, 30 °C, magnetic field	>80	>80	—	—
This work	*A. ferrooxidans*	Pyrolyzed industrial LCO black mass	1% pulp, pH 2.0 / non-adjusted, 30 °C	64-70	57-72	52-79	81-100

5. Conclusions

This study demonstrates that *Acidithiobacillus ferrooxidans* can effectively bioleach critical metals from pyrolyzed industrial $LiCoO_2$-derived black mass under mild conditions. At 30 °C and 1% pulp density, substantial recoveries were achieved within 6-7 days, reaching 64-70% for Co, 57-72% for Ni, 52-60% for Li (increasing up to 79% without initial pH adjustment), and 81-100% for Cu. The recovery curves indicate that most dissolution occurred during the early leaching period, followed by a

© 2025 by the author(s). Distributed under a Creative Commons CC BY license.

Preprints.org (www.preprints.org) | NOT PEER-REVIEWED | Posted: 27 January 2026 doi:10.20944/preprints202601.1942.v1

plateau, suggesting depletion of readily accessible metal-bearing phases or emerging kinetic limitations.

The evolution of pH and the growth behaviour of the microorganism indicate that leaching performance is closely linked to the establishment of an active iron-oxidizing population and the resulting development of acidic and oxidizing conditions in the leachate. Increasing pulp density from 1% to 2% reduced dissolution rates and final recoveries, confirming solids loading as a primary constraint in batch operation. Initial pH adjustment was not essential to achieve high Co and Ni recovery at low pulp density, but it influenced Li behaviour, highlighting the importance of pH trajectory management when lithium co-recovery is targeted.

The results provide clear operating windows for further optimization and support the feasibility of bacterial bioleaching as a low-impact route for recovering Co, Ni, Li and Cu from industrial LCO black mass. Future work should focus on improving late-stage kinetics, increasing feasible pulp density, and assessing reactor configurations and process strategies suitable for scale-up and integration into industrial recycling flowsheets.

Supplementary Materials: The following supporting information can be downloaded at: Preprints.org, Figure S1: (a) XRD diffraction pattern of the black mass.; (b) XRD diffraction pattern of the bioleached residues.

Author Contributions: Conceptualization, K.K.; methodology, K.K., L.A.T and M.O.P.; software, K.K., L.A.T., E.C. and A.K.; validation, K.P., L.A.T. and G.L.; formal analysis, K.K., L.A.T. and E.C.; investigation, L.A.T., K.K. and A.K.; resources, M.O.P. and G.L.; data curation, K.K., L.A.T. and M.O.P.; writing—original draft preparation, K.K.; writing—review and editing, L.A.T., K.P., E.C., G.L and M.O.P.; visualization, K.K and A.K.; supervision, M.O.P.; project administration, M.O.P.; funding acquisition, G.L and M.O.P. All authors have read and agreed to the published version of the manuscript.

Funding: This research received no external funding.

Data Availability Statement: The data presented in this study are available on request from the corresponding author (Kyriaki Kiskira). The data are not publicly available because they form part of ongoing research activities.

Acknowledgments: Part of this work was presented at the 14th International Conference on Instrumental Methods of Analysis: Modern Trends and Applications (IMA 2025), Kefalonia, Greece, 14-17 September 2025.

Conflicts of Interest: The authors declare no conflicts of interest.

Abbreviations

The following abbreviations are used in this manuscript:

Abbreviation	Definition
AAS	Atomic Absorption Spectroscopy
CEJ	Chemical Engineering Journal
Co	Cobalt
CRM	Critical Raw Material
Cu	Copper
DoE	Design of Experiments
DSMZ	Deutsche Sammlung von Mikroorganismen und Zellkulturen (German Collection of Microorganisms and Cell Cultures)
EDS	Energy Dispersive Spectroscopy
ED-XRF	Energy-Dispersive X-ray Fluorescence
EU	European Union
Fe	Iron
HPLC	High-Performance Liquid Chromatography
LIB	Lithium-Ion Battery
LCO	Lithium Cobalt Oxide

© 2025 by the author(s). Distributed under a Creative Commons CC BY license.

Preprints.org (www.preprints.org) | NOT PEER-REVIEWED | Posted: 27 January 2026 doi:10.20944/preprints202601.1942.v1

Li	Lithium
LOI	Loss on Ignition
Mn	Manganese
Ni	Nickel
NTUA	National Technical University of Athens
OD_{600}	Optical Density at 600 nm
SEM	Scanning Electron Microscopy
UV–Vis	Ultraviolet–Visible (spectrophotometry)
WEEE	Waste Electrical and Electronic Equipment
XRD	X-ray Diffraction
XRF	X-ray Fluorescence
Zn	Zinc

References

1. Rautela, R.; Yadav, B.R.; Kumar, S. A Review on Technologies for Recovery of Metals from Waste Lithium-Ion Batteries. *J. Power Sources* **2023**, *580*, 233428.
2. Kiskira, K.; Plakantonaki, S.; Gerolimos, N.; Kalkanis, K.; Sfyroera, E.; Coelho, F.; Priniotakis, G. Life Cycle Optimization of Circular Industrial Processes: Advances in By-Product Recovery for Renewable Energy Applications. *Clean Technol.* **2026**, *8*(1), 5. https://doi.org/10.3390/cleantechnol8010005
3. Ma, X.; Meng, Z.; Bellonia, M.V.; Spangenberger, J.; Harper, G.; Gratz, E.; Olivetti, E.; Arsenault, R.; Wang, Y. The Evolution of Lithium-Ion Battery Recycling. *Nat. Rev. Clean Technol.* **2025**, *1*, 75-94.
4. Zhang, X.; Li, L.; Fan, E.; Xue, Q.; Bian, Y.; Wu, F.; Chen, R. Toward Sustainable and Systematic Recycling of Spent Rechargeable Batteries. *Chem. Soc. Rev.* **2018**, *47*, 7239-7302.
5. Psomopoulos, C.S.; Kalkanis, K.; Chatzistamou, E.D.; Kiskira, K.; Ioannidis, G.Ch.; Kaminaris, S.D. End of Life Treatment of Photovoltaic Panels: Expected Volumes up to 2045 in E.U. *AIP Conf. Proc.* **2022**, *2437*, 020084. https://doi.org/10.1063/5.0092332
6. Mansur, M.B.; Guimarães, A.S.; Petraniková, M. An Overview on the Recovery of Cobalt from End-of-Life Lithium-Ion Batteries. *Miner. Process. Extr. Metall. Rev.* **2022**, *43*, 489-509.
7. Mishra, G.; Jha, R.; Meshram, A.; Singh, K.K. A Review on Recycling of Lithium-Ion Batteries to Recover Critical Metals. *J. Environ. Chem. Eng.* **2022**, *10*, 108534.
8. Takahashi, V.C.I.; Botelho Junior, A.B.; Espinosa, D.C.R.; Tenório, J.A.S. Enhancing Cobalt Recovery from Li-Ion Batteries Using Grinding Treatment Prior to the Leaching and Solvent Extraction Process. *J. Environ. Chem. Eng.* **2020**, *8*, 103801.
9. Meshram, P.; Virolainen, S.; Abhilash; Sainio, T. Solvent Extraction for Separation of 99.9% Pure Cobalt and Recovery of Li, Ni, Fe, Cu, Al from Spent LIBs. *Metals* **2022**, *12*, 1056.
10. Aboulaich, A.; Yaden, A.; Elhalya, N.; Taylour, M.; Aqil, M.; Hdidou, L.; Dahbi, M.; Alami, J. Synthesis and Recyclability of Sheet-like Cobalt Carbonate Recovered from Spent Li-Ion Batteries Using a Simple Hydrometallurgy Process. *Sustainability* **2022**, *14*, 2552.
11. Cornelio, A.; Zanoletti, A.; Bontempi, E. Recent Progress in Pyrometallurgy for the Recovery of Spent Lithium-Ion Batteries: A Review of State-of-the-Art Developments. *Curr. Opin. Green Sustain. Chem.* **2024**, *46*, 100881.
12. Holzer, A.; Windisch-Kern, S.; Ponak, C.; Raupenstrauch, H. A Novel Pyrometallurgical Recycling Process for Lithium-Ion Batteries and Its Application to the Recycling of LCO and LFP. *Metals* **2021**, *11*, 1-22.
13. Bourtsalas, A.C.; Papadatos, P.E.; Kiskira, K.; Kalkanis, K.; Psomopoulos, C.S. Ecodesign for Industrial Furnaces and Ovens: A Review of the Current Environmental Legislation. *Sustainability* **2023**, *15*(12), 9436. https://doi.org/10.3390/su15129436
14. Botelho Junior, A.B.; Stopic, S.; Friedrich, B.; Tenório, J.A.S.; Espinosa, D.C.R. Cobalt Recovery from Li-Ion Battery Recycling: A Critical Review. *Metals* **2021**, *11*, 1999.
15. Ochsenkühn-Petropoulou, M.; Tsakanika, L.A.; Lymperopoulou, T.; Ochsenkühn, K.M.; Hatzilyberis, K.; Georgiou, P.; Stergiopoulos, C.; Serifi, O.; Tsopelas, F. Efficiency of Sulfuric Acid Leaching for the Recovery of Critical Metals from Greek Bauxite Residue. *Metals* **2018**, *8*, 915. https://doi.org/10.3390/met8110915

© 2025 by the author(s). Distributed under a Creative Commons CC BY license.

Preprints.org (www.preprints.org) | NOT PEER-REVIEWED | Posted: 27 January 2026 doi:10.20944/preprints202601.1942.v1

16. Strauss, M.L.; Diaz, L.A.; McNally, J.; Klaehn, J.; Lister, T.E. Separation of Cobalt, Nickel, and Manganese in Leach Solutions of Waste Lithium-Ion Batteries Using Dowex M4195 Ion Exchange Resin. *Hydrometallurgy* **2021**, *206*, 105757.
17. Álvial-Hein, G.; Mahandra, H.; Ghahreman, A. Separation and Recovery of Cobalt and Nickel from End-of-Life Products via Solvent Extraction Technique: A Review. *J. Clean. Prod.* **2021**, 297, 126592.
18. Hatzilyberis, K.; Tsakanika, L.-A.; Lymperopoulou, T.; Georgiou, P.; Kiskira, K.; Tsopelas, F.; Ochsenkühn, K.-M.; Ochsenkühn-Petropoulou, M. Design of an Advanced Hydrometallurgy Process for the Intensified and Optimized Industrial Recovery of Scandium from Bauxite Residue. *Chem. Eng. Process. Process Intensif.* **2020**, *155*, 108015. https://doi.org/10.1016/j.cep.2020.108015
19. Tsakanika, L.-A.; Panagiotatos, G.; Lymperopoulou, T.; Chatzitheodoridis, E.; Ochsenkühn, K.; Ochsenkühn-Petropoulou, M. Direct Phosphoric Acid Leaching of Bauxite Residue for Selective Scandium Extraction. *Metals* **2022**, *12*, 228. https://doi.org/10.3390/met12020228
20. Arnold, S.; Ruthes, J.G.A.; Kim, C.; Presser, V. Electrochemical Recycling of Lithium-Ion Batteries: Advancements and Future Directions. EcoMat 2024, 6, e12494.
21. Yu, L.; Bai, Y.; Belharouak, I. Recycling of Lithium-Ion Batteries via Electrochemical Recovery: A Mini-Review. *Batteries* **2024**, 10, p.337.
22. Roy, J.J.; Cao, B.; Madhavi, S. A Review on the Recycling of Spent Lithium-Ion Batteries (LIBs) by the Bioleaching Approach. *Chemosphere* **2021**, *282*, 130944.
23. Kiskira, K.; Lymperopoulou, T.; Tsakanika, L.-A.; Pavlopoulos, C.; Papadopoulou, K.; Ochsenkühn, K.-M.; Lyberatos, G.; Ochsenkühn-Petropoulou, M. Study of Microbial Cultures for the Bioleaching of Scandium from Alumina Industry By-Products. *Metals* **2021**, *11*(6), 951. https://doi.org/10.3390/met11060951
24. Kiskira, K.; Lymperopoulou, T.; Lourentzatos, I.; *et al.* Bioleaching of Scandium from Bauxite Residue Using Fungus *Aspergillus niger*. *Waste Biomass Valorization* **2023**, *14*, 3377-3390. https://doi.org/10.1007/s12649-023-02116-5
25. Alipanah, M.; Jin, H.; Zhou, Q.; Barboza, C.; Gazzo, D.; Thompson, V.; Fujita, Y.; Liu, J.; Anderko, A.; Reed, D. Sustainable Bioleaching of Lithium-Ion Batteries for Critical Metal Recovery: Process Optimization through Design of Experiments and Thermodynamic Modeling. *Resour. Conserv. Recycl.* **2023**, *199*, 107293.
26. Kiskira, K.; Tsakanika, L.A.; Kritikos, A.; Ntakanas, C.; Chatzitheodoridis, E.; Papadopoulou, K.; Lyberatos, G.; Ochsenkühn-Petropoulou, M. Bioleaching of critical metals from spent lithium cobalt oxide batteries using *Acidithiobacillus ferrooxidans*. In Proceedings of the 14th International Conference on Instrumental Methods of Analysis: Modern Trends and Applications, Kefalonia, Greece, 14-17 September 2025. https://doi.org/10.5281/zenodo.17305087
27. Panda, S.; Dembele, S.; Mishra, S.; Akcil, A.; Agcasulu, İ.; Hazrati, E.; Tuncuk, A.; Malavasi, P.; Gaydardzhiev, S. Small-Scale and Scale-Up Bioleaching of Li, Co, Ni and Mn from Spent Lithium-Ion Batteries. *J. Chem. Technol. Biotechnol.* **2024**. https://doi.org/10.1002/jctb.7609
28. Biswal, B.K.; Balasubramanian, R. Recovery of Valuable Metals from Spent Lithium-Ion Batteries Using Microbial Agents for Bioleaching: A Review. *Front. Microbiol.* **2023**, *14*, 1197081. https://doi.org/10.3389/fmicb.2023.1197081
29. Tonietti, L.; Esposito, M.; Cascone, M.; Barosa, B.; Fiscale, S.; Muscari Tomajoli, M.T.; Sbaffi, T.; Santomartino, R.; Covone, G.; Cordone, A.; Rotundi, A.; Giovannelli, D. Unveiling the Bioleaching Versatility of *Acidithiobacillus ferrooxidans*. *Microorganisms* **2024**, *12*(12), 2407. https://doi.org/10.3390/microorganisms12122407
30. Naseri, T.; Mousavi, S.M. Improvement of Li and Mn Bioleaching from Spent Lithium-Ion Batteries Using Step-Wise Addition of Biogenic Sulfuric Acid by *Acidithiobacillus thiooxidans*. *Heliyon* **2024**, *e37447*. https://doi.org/10.1016/j.heliyon.2024.e37447
31. Kazemian, Z.; Larypoor, M.; Marandi, R. Evaluation of Myco-Leaching Potential of Valuable Metals from Spent Lithium Battery by *Penicillium chrysogenum* and *Aspergillus niger*. *Int. J. Environ. Anal. Chem.* **2023**, *103*(3), 514-527. https://doi.org/10.1080/03067319.2020.1861605
32. Li, J., Xu, T., Liu, J. *et al.* Bioleaching metals from waste electrical and electronic equipment (WEEE) by *Aspergillus niger*: a review. *Environ Sci Pollut Res* **28**, 44622-44637 (2021). https://doi.org/10.1007/s11356-021-15074-z

© 2025 by the author(s). Distributed under a Creative Commons CC BY license.

Preprints.org (www.preprints.org) | NOT PEER-REVIEWED | Posted: 27 January 2026 doi:10.20944/preprints202601.1942.v1

33. Gu, J.; Nie, Y.; Li, Z.; Yang, K.; An, L.; Jiang, H.; Han, X.; Fu, Z.; Zhao, X. Efficient Bioleaching of Li from Waste Lithium-Iron Phosphate Batteries by Acidophilic Bacterial Consortium: Enrichment Condition, Li Recovery, and Brief Carbon Footprint Analysis. *Chem. Eng. J.* **2025**, *161450*. https://doi.org/10.1016/j.cej.2025.161450
34. Heydarian, A.; Mousavi, S.M.; Vakilchap, F.; Baniasadi, M. Application of a Mixed Culture of Adapted Acidophilic Bacteria in Two-Step Bioleaching of Spent Lithium-Ion Laptop Batteries. *J. Power Sources* **2018**, *380*, 105-116. https://doi.org/10.1016/j.jpowsour.2017.12.009
35. Premathilake, D.S.; Botelho Junior, A.B.; Tenório, J.A.S.; Espinosa, D.C.R.; Vaccari, M. Designing of a Decentralized Pretreatment Line for EOL-LIBs Based on Recent Literature of LIB Recycling for Black Mass. Metals **2023**, 13(2), 374. https://doi.org/10.3390/met13020374
36. Rudolph, M.; van den Boogaart, K.G.; et al. Mineralogy and Material Characterization of Black Mass from Industrial LIB Recycling-Implications for Process Optimization. Minerals Engineering **2021**, 171, 107080. https://doi.org/10.1016/j.mineng.2021.107080
37. Nazerian, M.; Bahaloo-Horeh, N.; Mousavi, S.M. Enhanced Bioleaching of Valuable Metals from Spent Lithium-Ion Batteries Using Ultrasonic Treatment. *Korean J. Chem. Eng.* **2023**, *40*, 584-593. https://doi.org/10.1007/s11814-022-1257-2
38. Dash, J.; Ojha, R.; Pradhan, D. Progress in Bioleaching and Its Mechanism: A Short Review. *Discov. Environ.* **2025**, ***3***, 238. https://doi.org/10.1007/s44274-025-00454-w
39. Morell, J.; Lao-Luque, C.; Solé-Sardans, M.; Ribas, D.; Guimerà, X.; Dorado, A.D. Closed-Loop Bioleaching for Mobile Phones from the Bioregeneration of the Leaching Agent to the Recovery of Metal: A Review. *J. Ind. Eng. Chem.* **2025**, *xx*, 104020. https://doi.org/10.1016/j.jiec.2025.04.020
40. Garcia, L.; Morell, J.; Lao, C.; Solé-Sardans, M.; Dorado, A.D. Metal Recovery from Discarded Lithium-Ion Batteries by Bioleaching Coupled with Minimal Mechanical Pre-Treatment. *Minerals* **2025**, *15*(6), 566. https://doi.org/10.3390/min15060566
41. Mandl, M.M.; Lerchbammer, R.; Gerold, E. Bioleaching of Lithium-Ion Battery Black Mass: A Comparative Study on *Gluconobacter oxydans* and *Acidithiobacillus thiooxidans*. *Metals* **2025**, *15*(10), 1112. https://doi.org/10.3390/met15101112
42. Chacana-Olivares, J.; Peceño, B.; Grageda, M.; *et al.* Lithium-Ion Battery Recycling: A Perspective on Key Challenges and Opportunities. *npj Mater. Sustain.* **2025**, *3*, 38. https://doi.org/10.1038/s44296-025-00083-7
43. Zhang, X.; Shi, H.; Tan, N.; Zhu, M.; Tan, W.; Daramola, D.; Gu, T. Advances in Bioleaching of Waste Lithium Batteries under Metal Ion Stress. *Bioresour. Bioprocess.* **2023**, *10*(1), 19. https://doi.org/10.1186/s40643-023-00636-5
44. Elander, B.E.; Jiang, M.; Fahrenbruch, M.; Li, W.; Momeni, B.; Wang, D. Recycling Li-Ion Battery Cathode Materials in Iron-Fueled, Low-Sulfate Cultures of *Acidithiobacillus ferrooxidans*. *ACS Sustainable Resour. Manage.* **2025**, *2*(9), 1760-1768. https://doi.org/10.1021/acssusresmgt.5c00259
45. Kim, J.; Nwe, H.H.; Yoon, C.S. Enhanced Bioleaching of Spent Li-Ion Batteries Using *A. ferrooxidans* by Application of External Magnetic Field. *J. Environ. Manag.* **2024**, *367*, 122012. https://doi.org/10.1016/j.jenvman.2024.122012
46. Hong, J.-H.; Kim, J.; Han, E.; Yang, S.-M.; Kim, H.-S.; Kim, J.; Yoon, C.S. Magnetic Field-Assisted Bioleaching of Cathode Materials from Spent Li-Ion Batteries Using *Acidithiobacillus ferrooxidans*. *Chemosphere* **2025**, *376*, 144303. https://doi.org/10.1016/j.chemosphere.2025.144303
47. Kiskira, K.; Papirio, S.; Mascolo, M.C.; Fourdrin, C.; Pechaud, Y.; van Hullebusch, E.D.; Esposito, G. Mineral Characterization of the Biogenic Fe(III)(Hydr)oxides Produced during Fe(II)-Driven Denitrification with Cu, Ni and Zn. *Sci. Total Environ.* **2019**, *687*, 401-412. https://doi.org/10.1016/j.scitotenv.2019.06.107

Disclaimer/Publisher's Note: The statements, opinions and data contained in all publications are solely those of the individual author(s) and contributor(s) and not of MDPI and/or the editor(s). MDPI and/or the editor(s) disclaim responsibility for any injury to people or property resulting from any ideas, methods, instructions or products referred to in the content.

© 2025 by the author(s). Distributed under a Creative Commons CC BY license.